Degree of Polarization-Based Data Filter for Fully Polarimetric Synthetic Aperture Radar

Degree of Polarization Based Data Filter for Fully Polarimetric Synthetic Aperture Radar

Fang Shang, *Member, IEEE,* Naoto Kishi, *Senior Member, IEEE,* and Akira Hirose, *Fellow, IEEE*

Abstract—This paper proposes a novel data filtering algorithm for fully polarimetric synthetic aperture radar based on the degree of polarization information. First, we define the homogeneity degree and polarization independence degree using the DoP information, and propose a feature plane to characterize the target feature. Second, employing the feature plane, we categorize the targets into three types, and assign specific filtering policy for each type to estimate the optimal filtering window sizes. Finally, the T-matrices of fully polarimetric SAR data are filtered using the windows with estimated optimal sizes. Compared with boxcar filter, refined Lee filter, scattering model based filter, and improved sigma filter in processing ALOS2-PALSAR2 data, the proposed DoP based algorithm presents the best filtering performance.

I. INTRODUCTION

Polarimetric synthetic aperture radar (PolSAR) system is highly expected in land target observation since it has all day and all weather observing capability, and can collect polarization state information of scattered wave [1]–[5]. In the PolSAR data interpretation field, data filter is necessary to provide pre-processed data with lower speckle noice and higher scattered information accuracy in order to further analyze [6]–[9]. As a result, researches on data filter development continuously arouse discussions [10]–[15].

Basically, there are two requirements for data filtering, i.e., deducing speckle noise for homogeneous area to make it 'smooth', and protecting structural details for inhomogeneous area to make it 'clear'. The general procedure of typical algorithms is that first distinguish inhomogeneous targets using boundary detection [11] or high brightness points detection [12], [15], and assign small windows to these targets, and then filter the remaining homogeneous targets with a fixed or equivalent large local window [10]–[15]. Two factors limit their performance theoretically. First, among almost all filtering algorithms, inhomogeneous targets are distinguished based on fluctuation of scattered powers. Highly spatially fluctuated scattered powers are treated as the sign indicating inhomogeneous targets. However,the fundamental physical feature to judge homogeneity is the fluctuation of scattering mechanism, whereas the fluctuation of scattered power is only a possible subsequent appearance. It means that an inhomogeneous area definitely has spatially fluctuated scattering mechanisms, but not always leads to observable spatially fluctuated scattered

Fang Shang and Naoto Kishi are with the Department of Computer and Network Engineering, University of Electro-Communications, 1-5-1 Chofugaoka, Chofu, Tokyo 182-0021, Japan. e-mail: shangfang@uec.ac.jp

Akira Hirose is with the Department of Electrical Engineering and Information Systems, The Tokyo University, 7-3-1 Hongo, Bunkyo-ku, Tokyo 113-8656, Japan

powers. Actually, in a PolSAR intensity image, sometimes the man-made targets, especially ones with high distributing density and small scale, are too subtle or blurry to be found by power based algorithms. Such power based algorithms are essentially extensions of conventional processes of optical images. However, unlike the optical imaging data which provides only scattered power information, there are sufficient scattering mechanism information in a fully polarimetric SAR data. Therefore, developing a data filter for fully polarimetric SAR based on the fundamental scattering mechanism fluctuation instead of the power fluctuation is required. Second, to deal with homogeneous targets, the existing algorithms have not found an effective physical criteria to discriminate optimal window sizes of different homogeneous targets. Overestimated or underestimated window size usually leads to scattering information loss.

In this work, we propose a novel data filtering algorithm based on the degree of polarization (DoP) information for fully polarimetric SAR. The potential of the DoP information for data interpretation has been proved in many works [16]–[20]. The depolarization of the scattered wave is the most direct and observable response caused by scattering-mechanism fluctuation. However, such information is entangled with other features, and cannot be directly extracted from conventional C/T matrix. Therefore, in our previous works, we proposed extracting the DoP information from the averaged Stokes vector. We subsequently found the close relationship between the DoP curve and the optimal window size of data filtering [17], [18], [21]. Based on those pre-test results, we propose the complete data filtering algorithm. First, we define the homogeneity degree and polarization independence degree using the DoP information, and propose a feature plane. Next, by employing the feature plane, we categorize the targets into three types, and assign specific filtering policy for each type to estimate the optimal filtering window sizes. In order to enhance the robustness, we define fuzzy quadrants for the plane, i.e. there are no definite divisions among different types. If the corresponding point of a target is near to the fuzzy boundary of two types, both filtering policies of the two types will be considered comprehensively. Finally, for each pixel, the T-matrix is filtered using the estimated optimal window size particular for this pixel. In the proposed DoP based algorithm, inhomogeneous areas are distinguished according to the DoP fluctuations. The algorithm physically focuses on the scattering mechanism fluctuation to judge the homogeneity and can capture inhomogeneous areas with enhanced sensitivity. Moreover, the specific optimal window size for filtering each kind of homogeneous area is automatically determined by the

convergence feature of the DoP information. The proposed algorithm maximizes the protection of scattering information, which is highly useful in forest or vegetation observation that requires substantially more detailed information of homogeneous targets. In comparison with boxcar filter, refined Lee filter, scattering model based filter, and improved sigma filter in processing ALOS2-PALSAR2 data, the proposed DoP based algorithm presents the best filtering performance.

II. DEGREE OF POLARIZATION FOR DESCRIBING TARGET FEATURE

The key point of a data filtering algorithms is implementing different filtering policies to areas with different features. For a homogeneous area, a large window size is used to reduce speckle noise, whereas for an inhomogeneous area, a small window size is used to maintain spatial resolution. In order to characterize the target feature, we propose two parameters, i.e., the homogeneity degree, and the polarization dependency based on the DoP information.

A. Degree of Polarization of Fully Polarimetric SAR data

In previous works [17], [18] we have proposed the use of DoP for PolSAR data interpretation. Here, procedures of calculating DoP from Fully PolSAR data is reviewed.

Fully PolSAR system measures 2×2 complex scattering matrix S for each resolution element:

$$S = \left[\begin{array}{cc} S_{HH} & S_{HV} \\ S_{VH} & S_{VV} \end{array} \right] \quad (1)$$

where H and V represent horizontal and vertical polarization directions of antennas. In the case of backscattering in a reciprocal medium, $S_{HV} = S_{VH}$.

The scattering matrix relates the incident wave and the scattered wave. If we express the incident wave by a unit Jones vector $[E_H^i \ E_V^i]^T$, the scattered wave $[E_H^r \ E_V^r]^T$ can be obtained by

$$\left[\begin{array}{c} E_H^r \\ E_V^r \end{array} \right] = \left[\begin{array}{cc} S_{HH} & S_{HV} \\ S_{VH} & S_{VV} \end{array} \right] \left[\begin{array}{c} E_H^i \\ E_V^i \end{array} \right] \quad (2)$$

Then, the Jones coherency matrix J is defined as

$$J = \left[\begin{array}{cc} \langle E_H^r E_H^{r*} \rangle & \langle E_H^r E_V^{r*} \rangle \\ \langle E_V^r E_H^{r*} \rangle & \langle E_V^r E_V^{r*} \rangle \end{array} \right] = \left[\begin{array}{cc} J_{HH} & J_{HV} \\ J_{VH} & J_{VV} \end{array} \right] \quad (3)$$

where $\langle \cdot \rangle$ indicates spatial averaging process in a local window,i.e. data filtering. From the Jones coherency matrix, the averaged Stokes vector $\boldsymbol{G}$ is defined as

$$\boldsymbol{G} = \left[\begin{array}{c} g_0 \\ g_1 \\ g_2 \\ g_3 \end{array} \right] = \left[\begin{array}{c} J_{HH} + J_{VV} \\ J_{HH} - J_{VV} \\ J_{HV} + J_{VH} \\ j(J_{HV} - J_{VH}) \end{array} \right] \quad (4)$$

where j is the imaginary unit. Generally, this averaged Stokes vector expresses a partially polarized wave. Finally, the DoP can be calculated from the averaged Stokes vector as

$$\rho = \frac{\sqrt{g_1^2 + g_2^2 + g_3^2}}{g_0} \quad (5)$$

Since J is a complex Hermitian positive semidefinite matrix, it follows $g_1^2 + g_2^2 + g_3^2 \leq g_0^2$. So that, $0 \leq \rho \leq 1$.
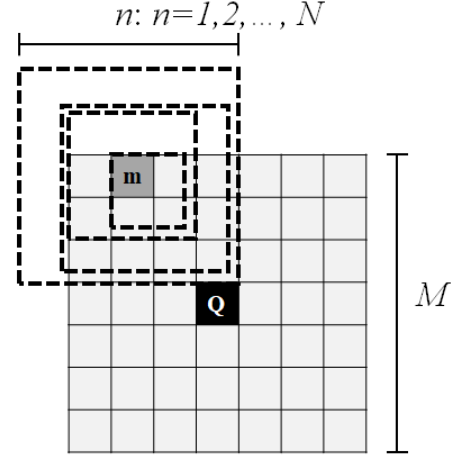

Fig. 1. Sketch of the $M \times M$ pixels sample area, and the $n \times n : n = 1, 2, \ldots, N$ pixels windows for calculating DoP information of $\mathbf{Q}$.

B. DoP Information of a Pixel

The DoP information describes the statistic characteristics of the scattering mechanisms in a local area. Therefore, in order to calculate the DoP information of a certain pixel $\mathbf{Q}$, the information of its nearby pixels is also needed. As shown in Fig. 1, pixels in an $M \times M$ sample area centered at $\mathbf{Q}$ will be considered in the calculation. For an arbitrary pixel m in this sample area, we can obtain a series of DoPs by using square windows with side lengths $n = 1, 2, \ldots, N$ to process spatial averaging in (3). Such a DoP series will be calculated for all of the pixels in the $M \times M$-pixel sample area. In the calculation, the supposed polarization state of the incident wave used in (2) is noted as [P]. Finally, we define the group of all these obtained DoP series the DoP information of pixel $\mathbf{Q}$ for polarization state [P]. Here, M should be big enough for observing the statistic characteristics of a local area, and N should be big enough for ensuring the convergence of the DoP series. In the calculation, square windows are used to easily ensure the windows with different sizes always having the same side-length ratio in azimuth and range directions.

As an example, in Fig. 2, we show the DoP information of ALOS2-PALSAR2 level 1.1 data of (a) a forest area, and (b) a city area, for horizontal polarized wave $[1 \ 0]^T$, vertical polarized wave $[0 \ 1]^T$, $45°$ linearly polarized wave $[1/\sqrt{2} \ 1/\sqrt{2}]^T$, and left circularly polarized wave $[1/\sqrt{2} \ j/\sqrt{2}]^T$. The parameters for calculating the DoP information are selected as $M = 11$, and $N = 20$. The figures show the averaged DoPs for each window size by black dots and the corresponding fluctuations by error bars. The fluctuation of the DoP information describing the neighboring situation is an important parameter to describe the feature of a local area. Here, we first define the accumulating fluctuation for polarization state [P] written as $\sigma_a^{[P]}$.

$$\sigma_a^{[P]} = \frac{1}{N} \sum_{n=2}^{N} E_n^{[P]} \quad (6)$$
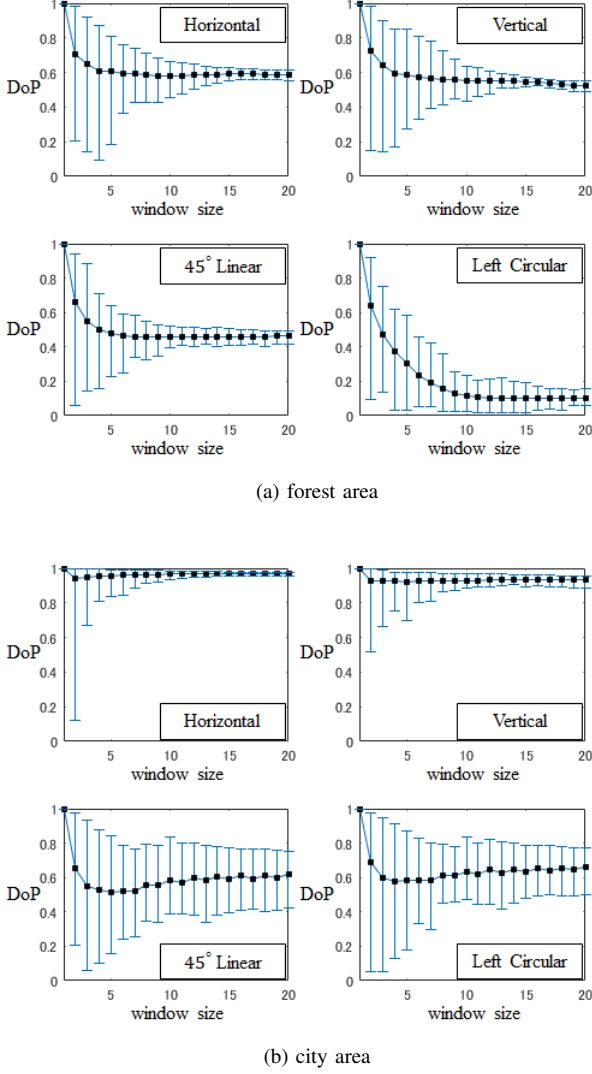
where

(a) forest area

(b) city area

Fig. 2. Polarization degrees versus calculation window size for (a) forest area, and (b) city area.

$$E_n^{[P]} = \max_{m=1,2,\ldots,M\times M}\{\text{DoP}_{n,m}^{[P]}\} - \min_{m=1,2,\ldots,M\times M}\{\text{DoP}_{n,m}^{[P]}\} \quad (7)$$

is the fluctuation range of DoPs calculated using $n \times n$ window size for polarization state [P] incident wave. Here $m = 1, 2, 3, \ldots, M \times M$ is index of all the samples. The parameter $\text{DoP}_{n,m}^{[P]}$ indicates the DoP of pixel m calculated with $n \times n$ window for [P] polarization state. Note that DoP with 1×1 window size is not used in the calculation. The reason is that DoP for a single pixel is always 1, and the corresponding fluctuation range is always 0 for any sample group. It is meaningless for evaluating the fluctuation.

Based on the accumulating fluctuation, we propose two parameters, i.e., the homogeneity degree and the polarization independence degree, to characterize the target feature.

C. Homogeneity Degree Described by the DoP Information

Homogeneity degree describes the fluctuation level of a certain physical parameter. Subsequently, the accumulating fluctuation of DoP defined above carries homogeneity information of this area. Based on this physical meaning, we can have an inference that if an observed area is inhomogeneous, high accumulating fluctuation should occur. We show this inference in Fig. 2. Observing the fluctuations in Fig. 2, we can find that for the forest area, i.e., an area with high homogeneity degree, the fluctuation ranges converge quickly with window size increasing. Subsequently, the accumulating fluctuations for the four kinds of polarization states will be low. Contrarily, for the city area, i.e., an area with low homogeneity degree, the fluctuation ranges of DoP for $45°$ linearly polarized, and left circularly polarized incident are large and not convergent. Correspondingly, the accumulating fluctuation for these two polarization states are high.

The example shows that for an inhomogeneous area, high accumulating fluctuations will really occur, but may only for some certain polarization states. Therefore, we use the maximum one of accumulating fluctuations for four types of polarization state to estimate the homogeneity degree. We propose the homogeneity degree D_{homo} as follows

$$D_{\text{homo}} = 1 - f_h(\sigma_a^{\text{max}}) \quad (8)$$

where $\sigma_a^{\text{max}} = \max\{\sigma_a^{[H]}, \sigma_a^{[V]}, \sigma_a^{[45°]}, \sigma_a^{[lc]}\}$. The superscripts [H], [V], [45°], and [lc] represent that the incident waves are horizontal polarized, vertical polarized, $45°$ linearly polarized, and left circularly polarized, respectively. The function $f_h(\cdot)$ is defined as

$$f_h(x) = \frac{1}{2}\tanh(10(x - \frac{1}{2})) + \frac{1}{2} \quad (9)$$

which is used for rescaling the maximum accumulating fluctuation σ_a^{max} in (8). The function $y = f_h(x)$ is a transformation of function $y = \tanh(x)$. It has a value range $y \in (0, 1)$ and a symmetric center $(x = 0.5, y = 0.5)$. The parameter 10 is used to ensure y can be sufficiently close to 1 when $x = 1$, whereas sufficiently close to 0 when $x = 0$. After rescaling the maximum accumulating fluctuation $\sigma_a^{\text{max}} \in [0, 1]$ by $f_h(\cdot)$, the values of $f_h(\sigma_a^{\text{max}})$ will approach to 1 if $\sigma_a^{\text{max}} > 0.5$, will approach to 0 if $\sigma_a^{\text{max}} < 0.5$, and will be 0.5 if $\sigma_a^{\text{max}} = 0.5$. Such a rescaling enhance the sensitivity of D_{homo} by enlarging the differences between homogeneous areas ($\sigma_a^{\text{max}} < 0.5$) and inhomogeneous areas ($\sigma_a^{\text{max}} > 0.5$). According to (8) and (9), the homogeneity degree D_{homo} satisfies $0 < D_{\text{homo}} < 1$. If an area is highly homogeneous, D_{homo} is close to 1, on the contrary, if an area is highly inhomogeneous, D_{homo} is close to 0.

Note that, in the proposed algorithm, the homogeneity of a local area is described according to the fluctuation of the scattering mechanisms essentially. In most of the other filtering algorithms, that is characterized based on the fluctuation of the scattered powers. However, the scattering mechanism fluctuation is the fundamental information, whereas the scattered power fluctuation is only a possible subsequent appearance. An inhomogeneous area has fluctuated scattering mechanisms. It usually leads to fluctuated scattered powers, but not always be obviously observable. Different from optical imaging data, in fully polarimetric SAR data, we have sufficient scattering
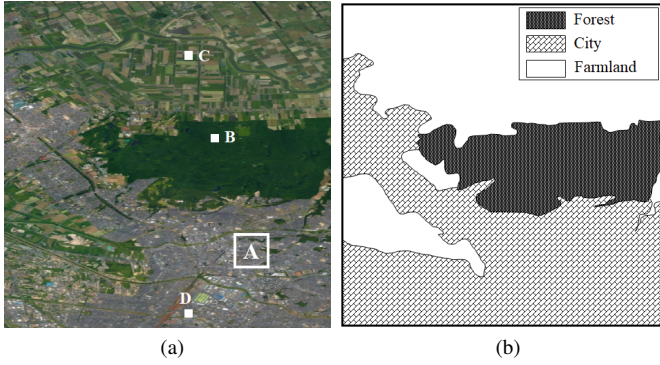
Fig. 3. (a) Google satellite photo of Ebetsushi area and patches used in evaluations, and (b) the sketch of the photo.

Fig. 4. Physical meanings of the feature plane exampled by Ebetsushi area.

mechanism information. Therefore, focusing on the scattering mechanism to judge the target feature is a better way.

D. Polarization Independence Degree Described by the DoP Information

Polarization dependency is another important parameter to characterize the target feature. It describes whether does the observed feature depend on the polarization state of the incident wave. The accumulating fluctuation also carries such a information. For example, in Fig. 2a, for a forest area, the fluctuations for four types of polarization states are almost the same. On the contrary, in Fig. 2b, for city area (here the data is selected from city with large buildings orthogonal to radar illumination), the fluctuations for horizontal polarized, vertical polarized incident waves are very low, whereas those for $45°$ linearly polarized, and left circularly polarized incident waves are very high.

We use the maximum one and the minimum one of accumulating fluctuations for four types of polarization state to estimate the polarization dependency. We propose the polarization independence degree D_{ind} as follows.

$$D_{\mathrm{ind}} = f_p \left(\frac{\sigma_a^{\min}}{\sigma_a^{\max}} \right) \quad (10)$$

where, similar to the definition of $\sigma_a^{\max}$, $\sigma_a^{\min} = \min\{\sigma_a^{[\mathrm{H}]}, \sigma_a^{[\mathrm{V}]}, \sigma_a^{[45°]}, \sigma_a^{[\mathrm{lc}]}\}$. The function $f_p(\cdot)$ is defined as

$$f_p(x) = x^{\frac{3}{2}} \quad (11)$$

which is used for rescaling the ratio $\sigma_a^{\min}/\sigma_a^{\max}$ in (10). After rescaling $\sigma_a^{\min}/\sigma_a^{\max}$ by $f_p(\cdot)$, we have values $D_{\mathrm{ind}} \in [0,1]$. A higher value indicates a higher independence degree. If the observed scattering feature of an area obviously depends on the polarization state of the incident wave, i.e., $\sigma_a^{\min}/\sigma_a^{\max} < 0.6$, D_{ind} is lower than 0.5. Otherwise, D_{ind} is higher than 0.5.

E. Feature Plane Defined by the Homogeneity Degree and Polarization Independence Degree

Based on the homogeneity degree and polarization independence degree proposed above, we define a feature plane for fully polarimetric SAR data. The homogeneity degree
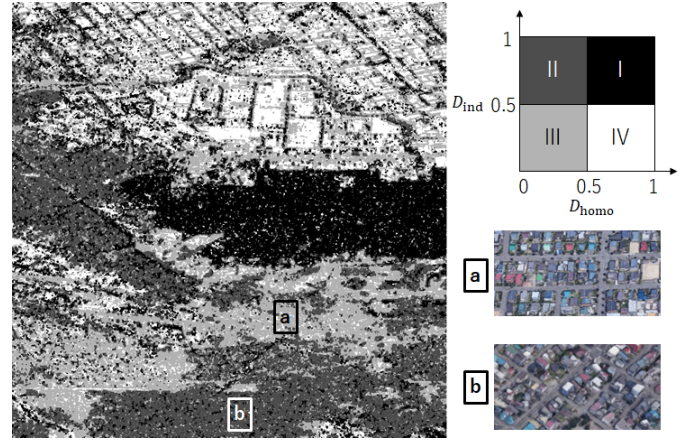
and polarization independence degree of each pixel can be expressed by a point, named feature point, in the feature plane. Here, ALOS2-PALSAR2 level 1.1 data for Ebetsushi area in Japan includes 3000×3000 pixels is used for showing the physical meanings of the plane. The Google map of Ebetsushi area and its land cover sketch is shown in Fig. 3. The parameters for calculating the DoP information are selected as $M = 11$, and $N = 15$. The test result is shown in Fig. 4. In the result, each pixel is expressed by the color corresponding to the quadrant which its feature point falls in. The colors for four quadrants are shown in the right part of Fig. 4. The feature points roughly distribute as follows.

1) Quadrant I ($D_{\mathrm{homo}} > 0.5$ and $D_{\mathrm{ind}} > 0.5$): Feature points of naturally growing plants such as forest distribute in this quadrant. In a local area, scattering mechanism of a forest area in each pixel is similar, therefore it has high homogeneity degree. The branches have almost equally possibility growing in all the orientations, therefore, it is reasonable to have high polarization independence degree.

2) Quadrant II ($D_{\mathrm{homo}} < 0.5$ and $D_{\mathrm{ind}} > 0.5$): Feature points of city with skew aligned or randomly distributed buildings such as area b shown in Fig. 4 fall in this quadrant. A man-made area has complicated textures, therefore, it has low homogeneity degree. Since the building are skew aligned to radar illumination, there is no strong double bounce scattering mechanism, i.e. the incident wave with any type of polarization state will be randomly scattered from the building surfaces. Therefore, it has high polarization independence degree.

3) Quadrant III ($D_{\mathrm{homo}} < 0.5$ and $D_{\mathrm{ind}} < 0.5$): Feature points of city with buildings orthogonal to radar illumination as area a shown in Fig. 4 fall in this quadrant such. Similar to the analysis of Quadrant II, such man-made area has low homogeneity degree. Such a man-made area leads to strong double bounce scattering. Ratio of the scattering coefficient for horizontal polarized wave, to the scattering coefficient for vertical polarized incident waves depends on material of the scatterer. If we only observe the DoP for horizontal polarized or vertical polarized wave, the DoP information of each sample should be similar because of the normalization in (5). However, if we observe DoP for $45°$ linearly polarized or left circularly polarized incident wave, which can be treated
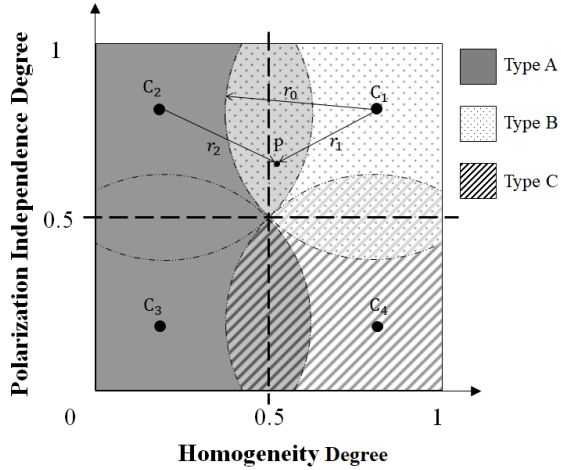
Fig. 5. Fuzzy quadrants of the feature plane for optimizing local filtering window size.

as a combination of a horizontal and a vertical polarized wave, the DoP information will be very different in each pixel because of the various scattering coefficient ratio. Therefore, it has low polarization independence degree.

4) Quadrant IV ($D_{\mathrm{homo}} > 0.5$ and $D_{\mathrm{ind}} < 0.5$): Feature points of farmland distribute in this quadrant. Similar to forest area, a farmland area has high homogeneity degree. However, unlike forest area, the shape configurations of crops are obviously oriented. It means that crops have obviously different responds to incident wave with different polarization states. Therefore, it has low polarization independence degree.

The test results above show that the feature plane have highly reasonable physical meaning. It is effective to characterize the target feature.

III. DEGREE OF POLARIZATION BASED FILTER

In this section, employing the feature plane, we propose a novel data filter for fully Polarimetric SAR.

A. Fuzzy Quadrants of Feature Plane

In many works [10], [21], [22], it has been shown that the optimal filtering window sizes for different types of areas are different. Therefore, we need to categorize the target, and assign specific window size optimizing policy to each type of targets. Using the four quadrants discussed in II-E to classify the feature points is a direct solution for this task. However, such definitely divided quadrants are not robust enough. For example, if the homogeneity degree is near to 0.5, it is difficult to say the target is homogeneous or inhomogeneous. Similar problem exists in the use of polarization dependence degree.

In order to enhance the robustness, we propose fuzzy quadrants for the feature plane as shown in Fig. 5. Boundaries of fuzzy quadrants are circular arcs centered at $C_1 : (0.8, 0.8)$, $C_2 : (0.2, 0.8)$, $C_3 : (0.2, 0.2)$, and $C_4 : (0.8, 0.2)$ with radius $r_0 = 3\sqrt{2}/10$. According to Fig. 5, neighboring quadrants in horizontal or vertical direction have an overlapping area, whereas quadrants in diagonal or off-diagonal direction do

not overlap each other. The fuzzy quadrants corresponds to three types of targets as shown in Fig. 5. Specific window size optimizing policy will be used for each type. However, if a feature point fall in the overlapping area of two types, which is named fuzzy type, policies of these two types will be considered simultaneously.

B. Optimal Filtering Window Size

The window size optimizing policies for three types and the fuzzy type are as follows.

1) Type A: fuzzy quadrants centered at C_2 and C_3 correspond to Type A. This type generally represents inhomogeneous areas. Therefore small window sizes should be used to protect detail shapes. Here we use square windows. The side length of optimal filtering window for a Type A target, written as L_{op}^A, is defined as

$$L_{\mathrm{op}}^A = \lceil 10 D_{homo} \rceil \tag{12}$$

where $\lceil x \rceil$ represents ceiling function which maps a real number x to the least integer greater than or equal to x. For example, if $D_{homo} = 0.35$, the side length of optimal filtering window is $L_{\mathrm{op}}^A = 4$, i.e., the optimal window size for filtering is 4×4.

2) Type B: fuzzy quadrant centered at C_1 corresponds to Type B. This type generally represents homogeneous areas with high homogeneity degree and high polarization independence degree. For such homogeneous areas, large window size is needed to decrease speckle noise. In [17], we determined optimal filtering window size by searching the smallest window size, with which the averaging DoP curve for $45°$ linearly polarized incident wave approached stable value. Employing the same method, we have shown in [21] that specific optimal window size can be effectively determined for different kinds of target areas. However, in recent research, we found that the averaging DoP curve based algorithm is sometimes not reliable. For example, in Fig. 2a, averaging DoP curve for $45°$ linearly polarized incident wave starts to be stable at 5×5 window size, i.e., the optimal window size determined by the method in [17] is 5×5. However, at 5×5 window size, the fluctuation of DoP is still large. The fluctuations start to be stable at around 10×10 window size. It means that the actual optimal window size, which ensure all the neighboring pixels can be effectively filtered, is 10×10. The window size is underestimated by averaging DoP curve based algorithm. Moreover, only $45°$ linearly polarized incident wave being considered in algorithm can not sufficiently use DoP information. Therefore, here we propose a new algorithm for searching optimal filtering window size for homogeneous areas based on the DoP fluctuations. First we define the side length of optimal window size estimated for the $[P]$ polarization state incident wave, $L_s^{[P]}$, as

$$L_s^{[P]} = \arg\min_n \left\{ n \ \middle| \ E_n^{[P]} \le (1 + \epsilon)\delta_t^{[P]} \text{ or } E_n^{[P]} \le \delta \right\} \tag{13}$$

where $\delta_t^{[P]} = \frac{1}{5}\sum_{i=N-4}^{N} E_i^{[P]}$ indicates the fluctuation of tails of DoP curves. With $n \times n$ window size, if $E_n^{[P]} \le$

$(1 + \epsilon) \left(\frac{1}{5} \sum_{i=N-4}^{N} E_i^{[P]} \right)$ is satisfied, the DoP information can be treated as relatively being stable. Or, if $E_n^{[P]} \leq \delta$ is satisfied, it means that the fluctuation is already very low, the DoP fluctuation can be treated as absolutely being stable. Here, $\epsilon \in (0, 1)$ is a tolerance coefficient to judge the relevant level of DoP fluctuation, and $\delta \in (0, 1)$ is a threshold to judge the absolute level of DoP fluctuation. $L_s^{[P]}$ is the smallest side length satisfies the stability conditions. Note that here n cannot be 1, since fluctuation for window size 1×1 is always 0 which is meaningless for stability judgment.

For a Type B target, the polarization independence degree is high. Therefore, the DoP information for various incident waves will be all convergent with similar fluctuation levels. The final side length of optimal window size for a Type B target is an averaging of the side lengths estimated by the four kinds of incident waves. It is

$$L_{op}^B = \left\lceil \frac{1}{4} \left(L_s^{[H]} + L_s^{[V]} + L_s^{[45°]} + L_s^{[lc]} \right) \right\rceil \quad (14)$$

3) Type C: fuzzy quadrant centered at C_4 corresponds to Type C. This type generally represents homogeneous areas with high homogeneity degree and low polarization independence degree. As discussed in II-E, for a target with obviously oriented configurations, though DoP information for various incident waves will be all convergent, the accumulating fluctuations are different. Among all the DoP informations, the one with lower accumulating fluctuation corresponds to stronger scattered power, which can describe the area better. Therefore, first we search the polarization state of incident wave which corresponds the lowest accumulating fluctuation, $[P_{min}]$, as follows

$$[P_{min}] = \arg \min_{[P]} \left\{ \sigma_a^{[P]} \right\} \quad (15)$$

where $[P]$ is among [H], [V], [45°], and [lc]. The final side length of optimal window size for Type C area is defined as

$$L_{op}^C = L_s^{[P_{min}]} \quad (16)$$

4) Fuzzy Type: overlapping parts of fuzzy quadrants correspond to Fuzzy Type. This type has features of two neighboring types, therefore, optimal window sizes estimated from two types will be considered comprehensively. If a Fuzzy Type feature point such as point P in Fig. 5 falls in the overlapping part of fuzzy quadrants centered at C_p and C_q where $[p, q] \in \{[1, 2], [3, 4], [1, 4]\}$, we note the distances between the point and the centers as r_p and r_q such as r_1 and r_2 in Fig. 5. The optimal window sizes estimated by the fuzzy quadrant centered at C_p and C_q, which is obtained by correspondingly using algorithms for Type A, Type B or Type C, are noted as L_{op}^p and L_{op}^q, respectively. The final side length of optimal window size for Fuzzy Type is defined as

$$L_{op}^{Fuzzy} = \left\lceil w_{op}^p L_{op}^p + w_{op}^q L_{op}^q \right\rceil \quad (17)$$

Here w_{op}^p and w_{op}^q are
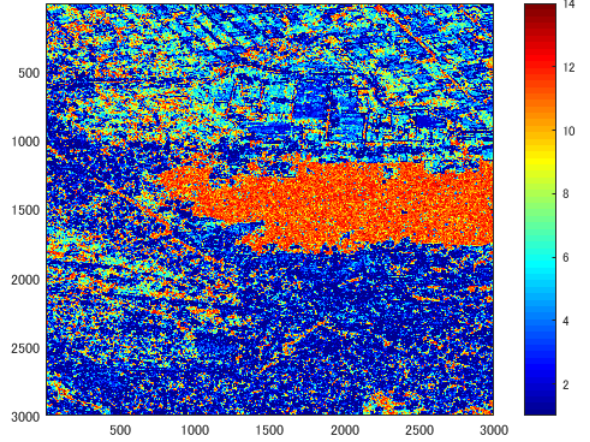

Fig. 6. Optimized local filtering window size with proposed algorithm for Ebetsushi area.

$$w_{op}^p = \frac{r_p - r_0}{(r_p - r_0) + (r_q - r_0)}$$
$$w_{op}^q = \frac{r_q - r_0}{(r_p - r_0) + (r_q - r_0)} \quad (18)$$

where r_0 is the radius of fuzzy quadrant as shown in Fig. 5.

With the algorithms described above, the estimated side length of optimal window for Ebetsushi area is shown in Fig. 6. The result shows that small window sizes (smaller than 4×4 pixels) are adaptively determined for city areas to protect detail shapes, whereas larger window size are adaptively determined for homogeneous areas such as farmland and forest to decrease speckle noise.

C. Data Filtering Procedure

For each pixel in the observation area, the data will be filtered by the corresponding optimal window size. Therefore, the data of the whole image is filtered using a moving window with a changing optimal window size. The data filtering process is implemented on coherency matrix, i.e., T matrix which is defined as

$$T = \boldsymbol{k} \cdot \boldsymbol{k}^{*T} \quad (19)$$

where $\boldsymbol{k} = \frac{1}{\sqrt{2}} [S_{HH} + S_{VV}, S_{HH} - S_{VV}, 2S_{HV}]^T$. Note a component of T matrix as t_{ij} where $i, j \in [1, 2, 3]$. The filtered component t_{ij}^f is calculated as

$$\tilde{t}_{ij} = \langle t_{ij} \rangle_{L_{op} \times L_{op}} \quad (20)$$

where $\langle \cdot \rangle_{L_{op} \times L_{op}}$ means spatial averaging in a $L_{op} \times L_{op}$ pixels local area.

Finally, the procedure of DoP based data filtering for a certain pixel **Q** is summarized as follows.

STEP 1: Calculate single look T matrix for all the pixels in observed area using equation (19). The calculated T matrices are waiting to be filtered.

(a) Google satellite photo

(b) boxcar filter

(c) refined Lee filter

(d) scattering model based filter

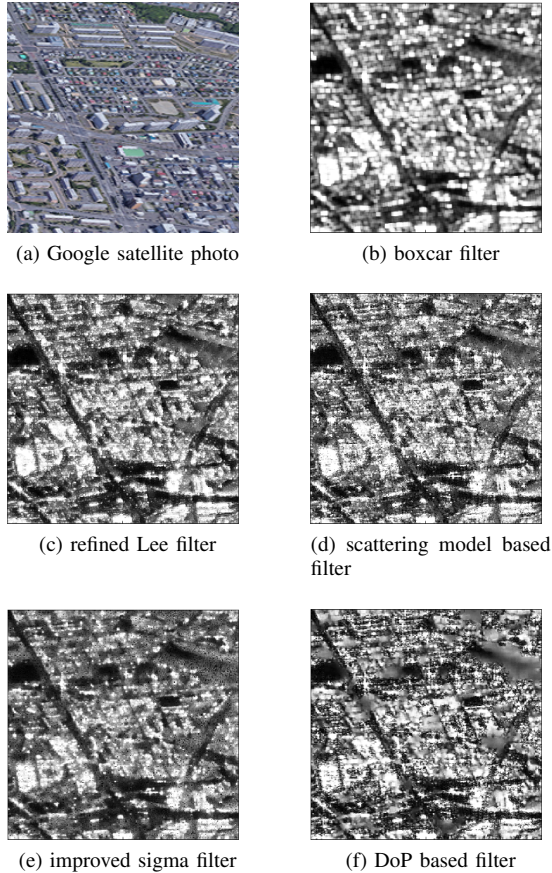(e) improved sigma filter

(f) DoP based filter

Fig. 7. (a) Google satellite photo of patch A, i.e., an highly inhomogeneous area, and span images of filtered T-matrix for the area obtained with (b) boxcar filter, (c) refined Lee filter, (d) scattering model based filter, (e) improved sigma filter, and (f) proposed DoP based filter.

STEP 2: For a certain pixel $\mathbf{Q}$ in the observed area as shown in Fig. 1, select the $M \times M$ pixels area centered at pixel $\mathbf{Q}$ for collecting neighboring pixels information.

STEP 3: For all the each pixel m included in the $M \times M$ pixels area as shown in Fig. 1, calculate $\mathrm{DoP}_{n,m}^{[P]}$ using equations (1) to (5), where $n = 1, 2, \ldots, N$ is side length of the square window size for calculating DoP, and $[P] \in \{[\mathrm{H}], [\mathrm{V}], [45°], [\mathrm{lc}]\}$ is the polarization states of incident waves. Therefore, for the pixel $\mathbf{Q}$, there are finally $N \times m \times m \times 4$ DoPs. The group of all these DoPs are the DoP information of the pixel $\mathbf{Q}$.

STEP 4: Using the DoP information of the pixel $\mathbf{Q}$, calculate the homogeneity degree D_{homo}, and the polarization independence degree D_{ind} according to equations (6) to (10).

STEP 5: Employing the feature plan with fuzzy quadrants shown in Fig. 5 to determine the target type of the $M \times M$ pixels area, and calculate side length of optimal window size, i.e., L_{op} for data filtering

    IF Type A: Calculate L_{op} using equation (12).

    IF Type B: Calculate L_{op} using equations (13) and (14).

    IF Type C: Calculate L_{op} using equations (15) and (16).

    IF Fuzzy Type: Calculate L_{op} using equation (17).

STEP 6: Filter each component of the T matrix for pixel $\mathbf{Q}$ by averaging the corresponding T matrix components in the

TABLE I

SPAN SD/M RATIOS OF FILTERED T-MATRIX IN HOMOGENEOUS AREAS OBTAINED WITH DIFFERENT FILTERS

	Patch B (forest)	Patch C (farmland)
Boxcar	0.229	0.304
Refined Lee	0.286	0.473
Scattering Model Based	0.513	0.618
Improved Sigma	0.550	0.326
DoP Based (proposed)	0.110	0.285

$L_{\mathrm{op}}^{\mathrm{TYPE}} \times L_{\mathrm{op}}^{\mathrm{TYPE}}$ local window centered at pixel $\mathbf{Q}$ according to equation (20).

IV. PERFORMANCE EVALUATION AND DISCUSSION

Here we compare the results with other adaptive filters for polarimetric SAR to evaluate the performance of the proposed degree of polarization based filter.

A. Filtering Algorithms for Comparison

Five filtering algorithms including the proposed one are used for comparison. All the filtering processes are implemented on T matrix. They are described as follows.

1) Boxcar filter: an algorithm filtering the data by averaging with a fixed window size. Here 5×5 boxcar filter is used for comparison.

2) Refined Lee filter: an algorithm employing boundary detection in each 7×7 local window. Here all the parameters are the same as those in [11].

3) Scattering model based filter: an algorithm classifying the pixels according to scattering model based decomposition before filtering. Here 9×9 window is used for testing, which is the same as described in [12].

4) Improved sigma filter: an algorithm based on bias compensation and dark pixels removal using sigma range. The algorithm is expended to apply for fully polarimetric SAR data in [15]. Here all the parameters are the same as those in [15].

5) The proposed DoP based filter: the proposed algorithm. Here the parameters used in the test are as follows. The area for testing neighboring information in (7) is $M \times M = 11 \times 11$, the largest window size for calculating DoP in (6) is $N \times N = 15 \times 15$, and the tolerance coefficient and threshold is $\epsilon = 20\%$ and $\delta = 0.2$, respectively, in (13).

B. Performance Evaluation for Ebetsushi Area

The first test data is ALOS2-PALSAR2 level 1.1 fully polarimetric SAR data for Ebetsushi area in Japan as shown in Fig. 3. First, we compare the effects of different filters on span of the filtered T matrices, which is defined as the summation of diagonal components, i.e.,

$$\mathrm{SPAN} = \tilde{t_{11}} + \tilde{t_{22}} + \tilde{t_{33}} \tag{21}$$

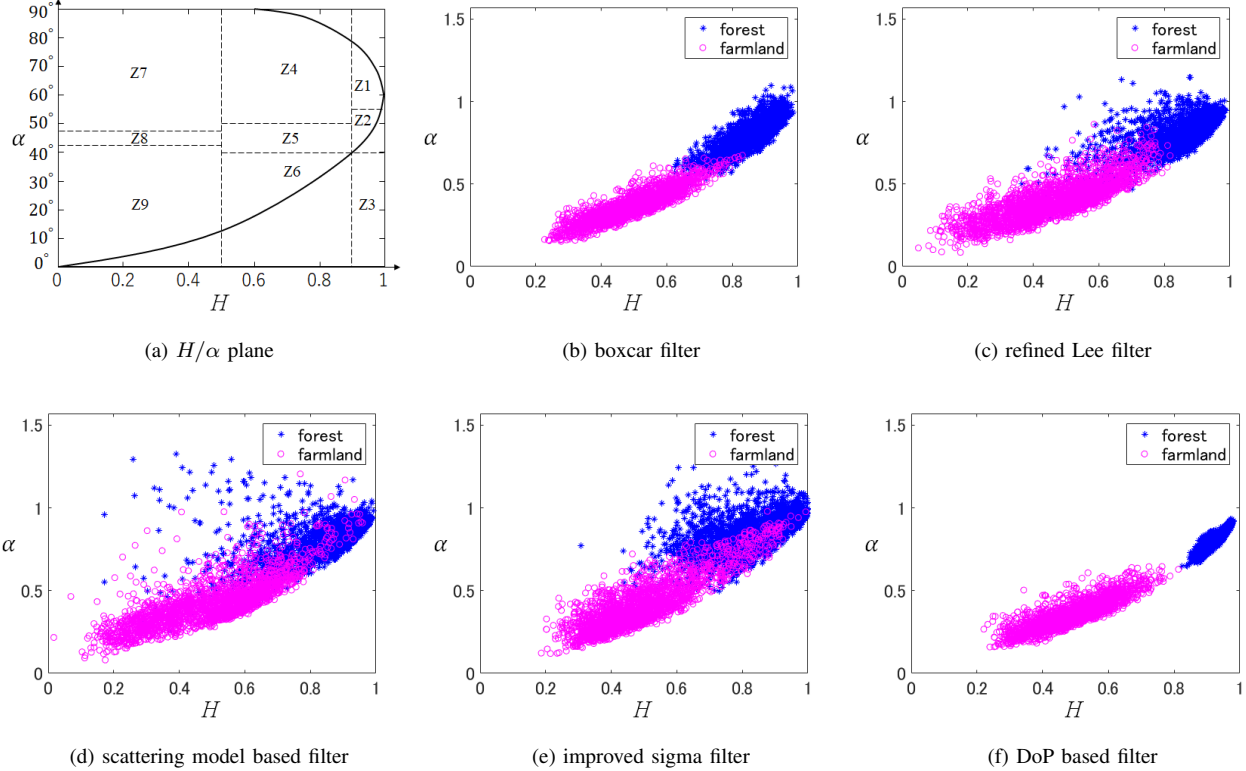The spans are compared in two aspects, i.e., performance on protecting detail shapes for inhomogeneous area, and

Fig. 8. (a) Sketch of H/α plane, and H/α point distributions for homogeneous areas, i.e., Patch B (farmland) and Patch C (forest) obtained with (b) boxcar filter, (c) refined Lee filter, (d) scattering model based filter, (e) improved sigma filter, and (f) proposed DoP based filter.

performance on decreasing speckle noise for homogeneous area. A 300×300 pixels city area is selected as shown by patch A in Fig. 3a to test the performance on protecting detail shapes for inhomogeneous area. The comparison results are shown in Fig. 7. The results shown that the proposed DoP based method leads to the least blur. A Forest area and a farmland area with 50×50 pixels as shown by patch B and patch C in Fig. 3a are selected to test the performance on decreasing speckle noise for homogeneous area. Standard deviation to the mean (SD/M) ratios are calculated for all the filtered data. The comparison results are shown in Table I. We can find that the proposed DoP based method has the lowest SD/M ratio for both of the forest and the farmland areas. Therefore, the proposed DoP based method shows highest performance on protecting detail shapes for inhomogeneous area, and decreasing speckle noise for homogeneous area.

The filtering effect on span is only one-side of the performance of filter. The main application of PolSAR data is interpreting scattering mechanisms of target using polarization information. Therefore, it is necessary to test whether the filtered T matrix can provide good interpreting performance. First, we compare the results generated by H/α method proposed in [9] with data filtered by different algorithms. The homogeneous areas patch B (forest) and patch C (farmland) in Fig. 3a are used in the test. The comparison results are shown in Fig. 8. The results show that, in the H/α plane, points corresponding to the T matrix filtered with the proposed algorithm provide the most clear division for the forest and the

farmland areas. Second, we compare the results generated by four-component scattered power decomposition with rotation proposed in [8] with data filtered by different algorithms. A forest area (patch B) and a city area (patch D) with 50×50 pixels are selected as samples for testing. The power contributions in four component decomposition algorithm for data filtered with different algorithms are shown in Table II. We can find that, for the forest area (patch B) and the city area (patch D), the result obtained with data filtered by proposed algorithm has the highest volume scattering proportion (82%) and highest double bounce scattering proportion (26%), respectively. The volume scattering is an important index to characterize forest areas, whereas the double bounce scattering is an important index to characterize man-made targets. Therefore, the results mean that the data filtered by the proposed algorithm can provide more accurate scattering information to component decomposition. Note that here patch D is a city area with small scale buildings, and the buildings are distributed skew aligned. The scattering mechanism of such areas include significant volume scattering, therefore, it is always difficult to distinguish such areas from volume scattering dominated forest areas [23], [24]. Increasing double bounce scattering of such man-made target areas in data filtering procedure is highly meaningful for data interpretation.

The comparison above show that the data filtered by the proposed DoP based algorithm provides scattering information with highest accuracy to further data interpretation procedure.

TABLE II
POWER CONTRIBUTIONS IN FOUR COMPONENT DECOMPOSITION
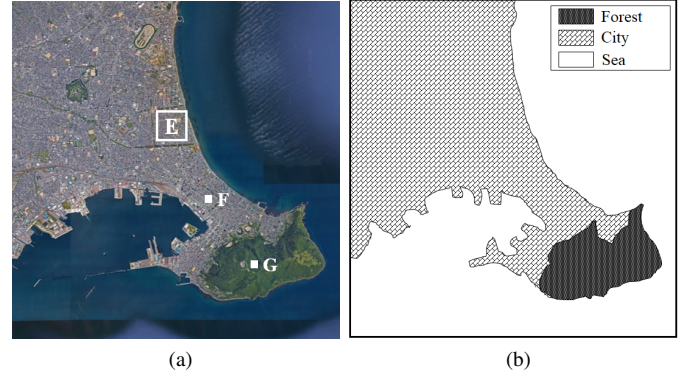OBTAINED WITH DIFFERENT FILTERS

Fig. 9. (a) Google satellite photo of Hakodate area and patches used in evaluations, and (b) the sketch of the photo.
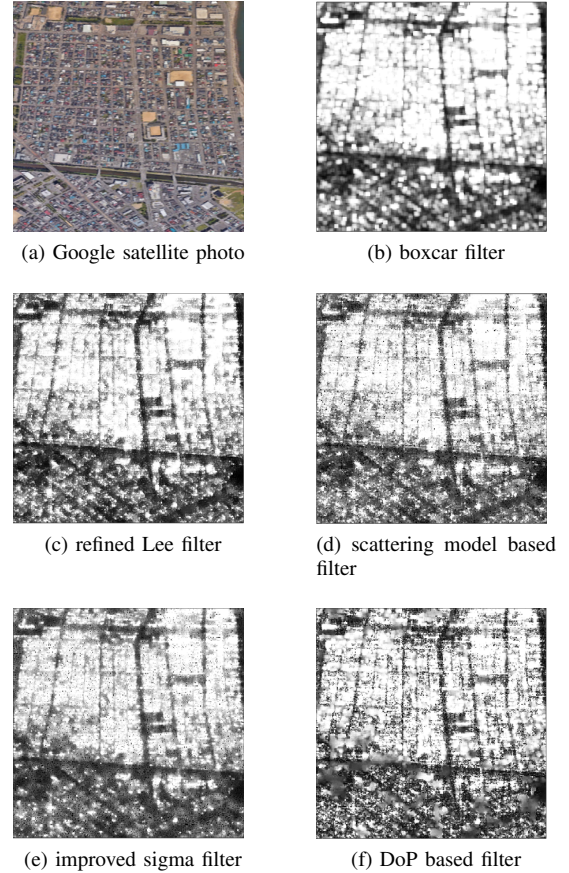

Fig. 10. (a) Google satellite photo of patch E, i.e., an highly inhomogeneous area, and span images of filtered T-matrix for the area obtained with (b) boxcar filter, (c) refined Lee filter, (d) scattering model based filter, (e) improved sigma filter, and (f) proposed DoP based filter.

C. Performance Test for Hakodate Area

The second test data is ALOS2-PALSAR2 level 1.1 fully polarimetric SAR data for Hakodate area in Japan as shown in Fig. 9. A 300×300-pixel city area is selected as shown by patch E in Fig. 9a to test the performance on protecting detail shapes for inhomogeneous area. The comparison results are shown in Fig. 10. The proposed DoP based method has the highest performance on protecting the detail shapes for inhomogeneous targets. A small city area and a forest area with 50×50 pixels as shown by patch F and patch G in Fig. 9a are selected for quantitative tests. The result is summarized in Table III. We can find that, for the city area (patch F), the result obtained with data filtered by the proposed algorithm has the highest double bounce scattering proportion (31.1%), whereas, for the city area (patch G), the result obtained with data filtered by our algorithm has the highest volume scattering proportion (76.8%). The SD/M ratios of the spans of data filtered with

different algorithms for patch G is also shown in Table III. The data filtered by the proposed method has the lowest SD/M ratio (0.207). The results show that the proposed algorithm provides the highest performance in comparison with other filters.

D. Discussion

In comparison with boxcar filter, refined Lee filter, scattering model based filter, and improved sigma filter, the proposed

TABLE III
POWER CONTRIBUTIONS IN FOUR COMPONENT DECOMPOSITION AND SPAN SD/M RATIOS OBTAINED WITH DIFFERENT FILTERS.

		Double Bounce	Volume	Surface	Helix	SD/M Ratio
Patch F (city)	Boxcar	23.5%	44.1%	26.9%	5.5%	-
	Refined Lee	27.0%	36.8%	29.0%	7.2%	-
	Scattering Model Based	25.5%	38.1%	30.0%	6.4%	-
	Improved Sigma	24.9%	41.7%	26.9%	6.5%	-
	DoP Based (proposed)	31.1%	30.0%	32.1%	6.8%	-
Patch G (forest)	Boxcar	9.7%	64.1%	18.1%	8.1%	0.323
	Refined Lee	11.0%	58.5%	21.5%	9.0%	0.379
	Scattering Model Based	11.9%	59.3%	21.1%	7.7%	0.434
	Improved Sigma	16.0%	48.2%	26.8%	9.0%	0.507
	DoP Based (proposed)	6.4%	76.8%	12.0%	4.8%	0.207

DoP based filter has the highest performance. The reason is its uniqueness on distinguishing inhomogeneous areas and determining optimal window size for homogeneous areas.

1) Uniqueness on Distinguishing Inhomogeneous Areas: The key point of all the data filtering algorithms is implementing different filtering policies to homogeneous area and inhomogeneous area. Therefore, whether a filter can distinguish inhomogeneous with high accuracy has significant influence on final performance of the filter. Until now, many algorithms are introduced to distinguish inhomogeneous targets such as boundary detection [11] and high brightness points detection [12], [15] based on the scattered power fluctuation information. However, the edges of some man-made targets, especially ones with high distributing density and small scale, can be too subtle or blurry to be found by boundary detection. And, not all the inhomogeneous areas have strong reflection to be found by high brightness points detection. Therefore, those algorithms sometimes lose efficiency. In the proposed DoP based algorithm, inhomogeneous areas are distinguished by the scattering mechanism fluctuation. It is the fundamental information, whereas the scattered power fluctuation is only a possible subsequent appearance. With this information, the proposed filter can capture inhomogeneous areas completely.

2) Uniqueness on Determining Optimal Window Size for Homogeneous Areas: To decrease speckle noise, large enough window size is needed for filtering homogeneous areas. In most of the filtering algorithms, if scale of a homogeneous area is large enough including no boundary or high brightness point, it will be filtered with a fixed large window size [10]–[12], [15]. However, we have shown that the optimal window sizes for different homogeneous areas area different [21], [22]. For example, the optimal window size for farmland area is around 5×5 pixels to 8×8 pixels, whereas the optimal window size for forest area is usually larger than 10×10 pixels for ALOS2-PALSAR2 data. Therefore, with fixed window size, overestimated or underestimated of window size exist in conventional algorithms. This problem will cause scattering information losses. In the proposed DoP based algorithm, the optimal window sizes for filtering homogeneous areas are determined by the convergence feature of the DoP information. Using such a method, we can automatically find the specific optimal window size for each kind of homogeneous area. It

maximizes the protection of scattering information. In forest observation or vegetation observation applications which requires much more detail information of homogeneous targets, such a protection will be highly useful.

We should note here, in this work, we have taken man-made targets and natural targets as examples to discuss low and high homogeneity degree. However, in the filtering process, what kinds of targets will be judged as inhomogeneous/homogeneous targets highly depends on the spatial resolution of the sensor. For example, within a 15×15 pixels window for ALOS/ALOS2 systems, an area with small buildings are inhomogeneous. However, if the resolution is very high, such a window may cover only a part of a building (for example a part of a roof). Then, this part may be treated as a homogeneous target in the filtering. In this case, some other targets with smaller scales such as telegraph poles and trash cans will be determined as inhomogeneous targets.

V. CONCLUSION

In this work, we have proposed a novel data filtering algorithm based on degree of polarization information for fully polarimetric SAR. In comparisons with boxcar filter, refined Lee filter, scattering model based filter, and improved sigma filter employing ALOS2-PALSAR2 data for Ebetsushi and Hakodate areas, the proposed DoP based algorithm has shown the highest performance on protecting structural details for inhomogeneous targets and decreasing speckle noise for homogeneous targets. Moreover, the proposed algorithm has shown the potential to provide scattering information with higher accuracy to further data interpretation procedure.

REFERENCES

[1] S. R. Cloude and E. Pottier, "A review of target decomposition theorems in radar polarimetry," *IEEE Trans. Geosci. Remote Sens.*, vol. 34, pp. 498–518, 1996.

[2] J. S. Lee, W. M. Boerner, D. L. Schuler, T. L. Ainsworth, I. Hajnsek, K. P. Papathanassiou, and E. Luneburg, "A review of polarimetric SAR algorithms and their applications," *Journal of Photogrammetry and Remote Sensing*, vol. 9, pp. 31–80, 2004.

[3] R. Touzi, W. M. Boerner, J. S. Lee, and E. Lueneburg, "A review of polarimetry in the context of synthetic aperture radar: Concepts and information extraction," *Can. J. Remote Sensing*, vol. 30, pp. 380–407, 2004.

[4] R. Touzi, R. K. Raney, and F. Charbonneau, "On the use of permanent symmetric scatterers for ship characterization," *IEEE Trans. Geosci. Remote Sens.*, vol. 42, pp. 2039–2045, 2004.

[5] F. D. Frate, A. Petrocchi, J. Lichtenegger, and G. Calabresi, "Neural networks for oil spill detection using ERS-SAR data," *IEEE Trans. Geosci. Remote Sens.*, vol. 37, pp. 2249–2258, 1999.

[6] A. Freeman and S. L. Durden, "A three-component scattering model for polarimetric SAR data," *IEEE Trans. Geosci. Remote Sens.*, vol. 36, pp. 963–973, 1998.

[7] Y. Yamaguchi, T. Moriyama, M. Ishido, and H. Ymada, "Four-component scattering model for polarimetric SAR image decomposition," *IEEE Trans. Geosci. Remote Sens.*, vol. 43, pp. 1699–1706, 2005.

[8] Y. Yamaguchi, A. Sato, W. M. Boerner, R. Sato, and H. Yamada, "Four-component scattering power decomposition with rotation of coherency matrix," *IEEE Trans. Geosci. Remote Sens.*, vol. 49, pp. 2251–2258, 2011.

[9] S. R. Cloude and E. Pottier, "An entropy based classification scheme for land applications of polarimetric SAR," *IEEE Trans. Geosci. Remote Sens.*, vol. 35, pp. 68–78, 1997.

[10] F. K. Lang, J. Yang, and D. Li, "Adaptive-window polarimetric SAR image speckle filtering based on a homogeneity measurement," *IEEE Trans. Geosci. Remote Sens.*, vol. 53, pp. 5435–5446, 2015.

[11] J. S. Lee, M. R. Grunes, and G. Grandi, "Polarimetric SAR speckle filtering and its implication for classification," *IEEE Trans. Geosci. Remote Sens.*, vol. 37, pp. 2363–2373, 1999.

[12] J. S. Lee, M. R. Grunes, D. L. Schuler, E. Pottier, and L. Ferro-Famil, "Scattering-model-based speckle filtering of polarimetric SAR data," *IEEE Trans. Geosci. Remote Sens.*, vol. 44, pp. 176–187, 2006.

[13] J. Chen, Y. L. Chen, W. T. An, Y. Cui, and J. Yang, "Nonlocal filtering for polarimetric SAR data: A pretest approach," *IEEE Trans. Geosci. Remote Sens.*, vol. 49, pp. 1744–1754, 2011.

[14] F. K. Lang, J. Yang, D. R. Li, L. Shi, and J. J. Wei, "Mean-shift-based speckle filtering of polarimetric SAR data," *IEEE Trans. Geosci. Remote Sens.*, vol. 52, pp. 4440–4454, 2014.

[15] J. S. Lee, T. L. Ainsworth, and K. S. Chen, "Speckle filtering of dual-polarization and polarimetric sar data based on improved sigma filter," in *IGARSS*, 2008, pp. IV21–IV24.

[16] R. Touzi, S. Goze, T. L. Toan, A. Lopes, and E. Mougin, "Polarimetric discriminators for SAR images," *IEEE Trans. Geosci. Remote Sens.*, vol. 30, pp. 973–980, 1992.

[17] F. Shang and A. Hirose, "Quaternion neural-network-based polsar land classification in poincare-sphere-parameter space," *IEEE Trans. Geosci. Remote Sens.*, vol. 52, pp. 5693–5703, 2014.

[18] ——, "Averaged stokes vector based polarimetric sar data interpretation," *IEEE Trans. Geosci. Remote Sens.*, vol. 53, pp. 4536–4547, 2014.

[19] D. L. Evans, T. G. Farr, J. J. V. Zyl, and H. A. Zebker, "Radar polarimetry: Analysis tools and applications," *IEEE Trans. Geosci. Remote Sens.*, vol. 26, pp. 774–789, 1988.

[20] F. Shang and A. Hirose, "PolSAR land classification by using quaternion-valued neural networks," in *APSAR 2013*, to be presented.

[21] M. Sugita, N. Kishi, and F. Shang, "Automatic-zooming-type window size optimization for polsar data interpretation," in *IGARSS*, 2018, p. to appear.

[22] F. Shang and A. Hirose, "Combination use of multiple window sizes for stokes vector based polsar data interpretation," in *IGARSS*, 2017, pp. 3913–3916.

[23] Y. Cui, Y. Yamaguchi, J. Yang, H. Kobayashi, and S. E. Park, "On complete model-based decomposition of polarimetric SAR coherency matrix data," *IEEE Transactions on Geoscience and Remote Sensing*, vol. 52, pp. 1991–2001, 2014.

[24] G. Singh, Y. Yamaguchi, and S. E. Park, "General four-component scattering power decomposition with unitary transformation of coherency matrix," *IEEE Trans. Geosci. Remote Sens.*, vol. 51, pp. 3014–3022, 2013.

Fang Shang (M'15) received the B.S. and M.S. degree in electrical engineering and automation from Harbin Institute of Technology, China, in 2009 and 2011. She received the Ph.D degree in electrical engineering and information systems from The University of Tokyo, Japan, in 2014. Dr. Shang is an Assistant Professor in the Graduate School of Informatics and Engineering, University of Electro-Communications, Japan. Her current research interest is in the signal and imaging processing for the polarimetric SAR.
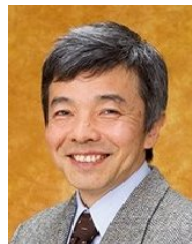
Naoto Kishi (SM'11) was born in Tokyo on 11 March, 1960. He received M.E. degree from the University of Electro-Communications(UEC), Tokyo, Japan, in 1984 and Ph.D. degree from the University of Tokyo, Tokyo, Japan, in 1987, respectively, all in electrical engineering. In 1987, he joined the Department of Electronic Engineering at the University of Electro-Communications(UEC) as a Research Associate. Currently, he is a Professor of the Department of Computer and Network Engineering, Faculty of Informatics and Engineering of UEC. In 1989 he was awarded the Abroad Research Scholarship by the Education Ministry of Japan. From April 1990 to September 1991, on leave from the University of Electro-Communications, he joined the Optoelectronics Research Centre at the University of Southampton, Southampton, England, as an Overseas Research Fellow, where he studied multiple quantum-well modulated optical fibre lasers and theory of acousto-optic modulator for fibre lasers. His main fields of interest are active and/or passive lightwave and microwave devices/systems, fibre-optic communication systems, numerical analysis in guided-wave optics, sensing systems using radio-wave and/or lightwave.

Dr. Kishi is a member of The Institute of Electronics, Information and Communication Engineers of Japan(IEICE), The Institute of Electrical and Electronics Engineers(IEEE), the Optical Society of Japan(OSJ), and the Optical Society of America(OSA). In 1989, he was a recipient of the fourth Shinohara Memorial Award by the IEICE.

Akira Hirose (F'13) received the Ph.D. degree in electronic engineering from the University of Tokyo in 1991. In 1987, he joined Research Center for Advanced Science and Technology (RCAST), the University of Tokyo, as Research Associate. In 1991, he was appointed as Instructor at RCAST. From 1993 to 1995, on leave of absence from the University of Tokyo, he joined the Institute for Neuroinformatics, University of Bonn, Bonn, Germany. He is currently Professor with the Department of Electrical Engineering and Information Systems, the University of Tokyo. The main fields of his research interests are wireless electronics and neural networks. In the fields, he published several books such as Complex-Valued Neural Networks, 2nd Edition (Springer 2012).

He served previously as the Founding President of Asia-Pacific Neural Network Society (APNNS) (2016), President of Japanese Neural Network Society (JNNS) (2013-2015), Vice President of the IEICE Electronics Society (ES) (2013-2015), Editor-in-Chief of the IEICE Transactions on Electronics (2011-2012), Associate Editor of journals such as the IEEE TRANSACTIONS ON NEURAL NETWORKS (2009-2011), IEEE GEOSCIENCE AND REMOTE SENSING NEWSLETTER (2009-2012), Chair of the Neurocomputing Technical Group in the IEICE, and General Chair of International Conference on Neural Information Processing (ICONIP) 2016 Kyoto and Asia-Pacific Conference on Synthetic Aperture Radar (APSAR) 2013 in Tsukuba. He currently serves as a member of IEEE Computational Intelligence Society (CIS) Neural Networks Technical Committee (NNTC) (2009-), Founding Chair of the NNTC Complex-Valued Neural Network Task Force (2010-), Governing Board Member of APNNA/APNNS (2006-), IEEE GRSS Tokyo Chapter Chair (2013-2015), and General Chair of International Geoscience and Remote Sensing Symposium (IGARSS) 2019 Yokohama.

Dr. Hirose is a Fellow of the IEEE, Senior Member of the IEICE, and a Member of JNNS and APNNS.